Coherent Control of the Exciton-Biexciton System in an InAs Self-Assembled Quantum Dot Ensemble

Takeshi Suzuki, Rohan Singh, Manfred Bayer, Arne Ludwig, Andreas D. Wieck, and Steven T. Cundiff

Phys. Rev. Lett. **117**, 157402 — Published 6 October 2016

DOI: 10.1103/PhysRevLett.117.157402

Coherent Control of the Exciton/Biexciton System in an InAs Self Assembled Quantum Dot Ensemble

Takeshi Suzuki[1,2], Rohan Singh[1,2], Manfred Bayer[3], Arne Ludwig[4], Andreas D. Wieck[4], and Steven T. Cundiff[1,2]
[1] *JILA, University of Colorado & National Institute of Standards and Technology, Boulder, Colorado 80309-0440, USA*
[2] *Physics Department, University of Michigan, Ann Arbor, MI 48109, USA*
[3] *Experimentelle Physik 2, Technische Universtät Dortmund, D-44221 Dortmund, Germany*
[4] *Lehrstuhl fuer Angewandte Festkoerperphysik, Ruhr-Universitaet Bochum, Universitaetsstrasse 150, D-44780 Bochum, Germany*
(Dated: September 7, 2016)

Coherent control of a strongly inhomogeneously broadened system, namely InAs self-assembled quantum dots, is demonstrated. To circumvent the deleterious effects of the inhomogeneous broadening, which usually masks the results of coherent manipulation, we use pre-pulse two-dimensional coherent spectroscopy to provide a size-selective readout of the ground, exciton and biexciton states. The dependence on the timing of the prepulse is due to the population dynamics of the coherently generated populations. To further validate the results, we performed pre-pulse polarization dependent measurements and confirmed the behavior expected from selection rules. All measured spectra can be excellently reproduced by solving the optical Bloch equations for a 4-level system.

PACS numbers: 78.67.Hc, 73.21.La, 78.47.jh

Coherent control uses the light-matter interaction to drive matter into a target final state. A key operation in many approaches to coherent control is a Rabi oscillation. While there are advantages to performing coherent control in ensembles because of their higher optical density and the presence of collective effects [1, 2], ensembles often display inhomogeneous broadening, which occurs when the resonance frequencies of the members of the ensemble fluctuate. Inhomogeneous broadening is deleterious for observing the occurrence of Rabi oscillations because the oscillation frequency depends on the detuning, resulting in a distribution of Rabi frequencies in an inhomogeneously broadened ensemble. Typically this problem is avoided by restricting demonstrations of coherent control to homogeneous ensembles or single objects. The effects of inhomogeneous broadening can also be circumvented by performing a Rabi rotation in a time shorter than the inverse of the inhomogeneous width, however that is often not practical due to the required intensities.

In this Letter, we demonstrate that Rabi oscillations in an inhomogeneously broadened system can be observed by using optical two-dimensional coherent spectroscopy to provide a probe that resolves the frequency groups within the inhomogeneous distribution, thus effectively removing the effects of inhomogeneous broadening and allowing the populations of the constituent frequency groups to be tracked separately. Furthermore, we are able to observe the coherent interplay between two states with an energetic splitting that is small compared to inhomogeneous width. This demonstration significantly extends the applicability of coherent control because many systems exhibit unavoidable inhomogeneity [3, 4], and thus were not previously candidates for coherent control.

Our approach is broadly applicable to inhomogeneously broadened ensembles. One example, which we choose for our demonstration, is semiconductor quantum dots (QDs), in which inhomogeneous broadening occurs due to the distribution in sizes and composition. While coherent control of single QDs has been studied due to the interest for quantum information processing [5–8], ensemble QDs have other potential applications such as QD lasers [9, 10], QD semiconductor amplifiers (SOAs) [11], and quantum memories [12]. Furthermore, coherent control of ensemble QDs can be a necessary ingredient for the implementation of large scale quantum bits [13]. A detailed understanding of the coherent light-matter interaction in ensemble QDs has been hindered by the presence of inhomogeneous broadening.

To overcome challenges due to inhomogeneity in QD ensemble systems, various optical techniques have been employed, such as spectral-hole burning [14], two-color spin noise spectroscopy [15], and transient four-wave mixing (FWM) [16, 17]. Recently, two dimensional coherent spectroscopy (2DCS) has been employed to study QD ensembles due to its advantage of unfolding the nonlinear signal into two frequency dimensions, enabling the isolation of the biexciton signal from the charged exciton (trion) signal [18], decoupling the homogeneous and inhomogeneous line widths [19], and spectrally resolving the homogeneous width, which provides insight into the effect of QD morphology on electronic properties [20, 21]. 2DCS overcomes the limitation of other conventional pump-probe techniques that spectrally average coherent light-matter interactions [22, 23].

While the ability of 2DCS to measure the variation of optical properties within the size distribution of QDs is already powerful, we take it to the next level by showing that it can reveal the coherent manipulation of the QDs

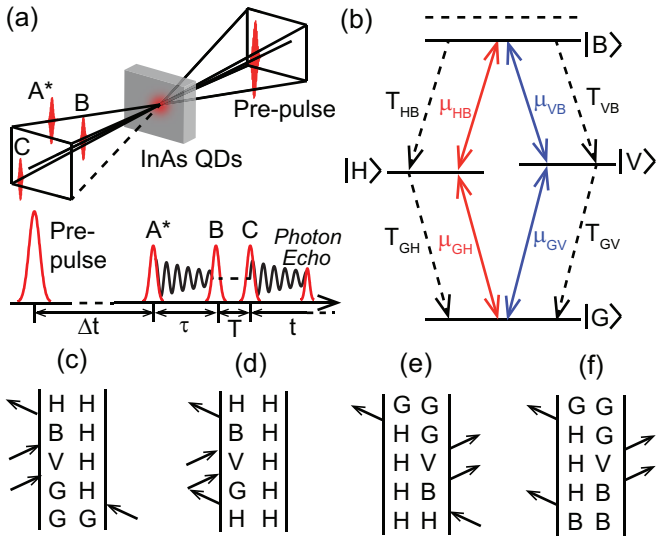

FIG. 1. (Color online) (a) Schematics of the pre-pulse 2DCS experiment for an InAs QD ensemble and time ordering. Delays between pre-pulse, A*, B, C, and signal are denoted as Δt, τ, T, t, respectively. (b) The energy level diagram showing the ground ($|G\rangle$), horizontal ($|H\rangle$) and vertical ($|V\rangle$) excitons, and biexciton ($|B\rangle$) states. The coherent paths for the interaction with the pre-pulse are shown as solid arrows and the radiative decay paths are shown as dashed arrows. (c-f) Double-sided Feynman diagrams representing all the quantum pathways [24] for cross-linear polarization, where (c), (d, e), and (f) start with population in the ground, H exciton, and biexciton states, respectively. The vertical lines represent evolution of the density matrix. The arrows in each diagram from the bottom to the top correspond to pulses A*, B, C, and signal, respectively.

despite the fact that it varies with size. Furthermore, we show that the population dynamics on coherently generated populations can be observed by changing the delay of the pre-pulse and interpret results as radiative decay representing the ultimate limit of coherence. Pre-pulse polarization results are in good agreement with selection rules.

Figure 1(a) is a schematic of the experiment. The pre-pulse and each pulse used in 2DCS have the same spectral profile and are generated by a mode-locked Ti:sapphire laser at a repetition rate of 76 MHz. The pulses have a bandwidth of 14.8 meV (full width at half maximum) as shown in the inset of Fig. 2(b). The spatial profile of the pre-pulse is twice as broad as the 2D pulses in order to reduce spatial inhomogeneity in excitation. 2DCS is an extension of the three-pulse transient FWM technique with the addition of interferometric stabilization of the pulse delays and measurement of the signal field [25]. Three pulses are incident on the sample in a rephasing (photon-echo) time-ordering, where the so-called conjugate pulse A* comes first, followed by pulses B and C. Delays between pulses A*, B, C, and the emitted FWM signal are denoted as τ, T, and t, respectively (Fig. 1(a)). A Fourier transform of the signal with respect to τ and t generates a 2D spectrum, in which the excitation and emission energies are correlated along the vertical and horizontal axes, respectively. Since the pulse A* is conjugate to the signal, the excitation energy is shown as negative values. The delay between the pre-pulse pump and the 2DCS probe (pulse A*) is denoted as Δt.

Figure 1(b) shows the energy level scheme of the InAs QD excitonic system. The two non-degenerate exciton states $|H\rangle$ and $|V\rangle$ have orthogonal linearly polarized transitions to the ground state $|G\rangle$ due to the cylindrical-symmetry breaking. The energy of the biexciton state $|B\rangle$ is lower than the sum of the two exciton energies by the biexciton binding energy of 3.3 meV [21, 26], which is much larger than the fine structure splitting energy of 19 μeV between $|H\rangle$ and $|V\rangle$ [27–29]. A key result of this work is simultaneous coherent control of both the biexciton state and the exciton state by using much broader spectrum for the pre-pulse than biexciton binding energy.

The sample is an InAs self-assembled QD ensemble with GaAs barriers, consisting of 10 quantum-mechanically-isolated epitaxially-grown layers. It is thermally annealed post-growth at 900 °C for 30 s, which results in a 100 meV in-plane confinement. The sample was unavoidably doped during growth, resulting in approximately half of the QDs being charged with a hole, which forms a trion with a photo excited electron and hole pair [18]. This doping occurred unintentionally, but at a known and reproducible level. The In content becomes reduced and distributed during sample growth and processing [30]. The maximum In content is estimated to reach 40 % in our sample. The sample is aligned such that the eigenstates are along the horizontal (H) and vertical (V) directions. All measurements are performed with the sample cooled at 10 K in a flow cryostat. The pre-pulse was focused to a diameter of 135 μm and QD density is 10^{10} /cm^2 per layer, which results in an excitation of $\sim 10^7$ QDs in the ensemble.

A cross-linearly polarized excitation and detection scheme is used, i.e. HVVH for A*, B, C and the signal, respectively, which isolates the biexciton signal from the trion's [21]. Figure 2(a) shows a 2D rephasing amplitude spectrum without the pre-pulse. The spectrum shows two peaks that are inhomogeneously broadened along the diagonal direction, indicated by dashed lines, due to QD size dispersion. The peak labeled Tr arises from the trion nonlinear response, whereas the peak labeled LP arises from the biexciton nonlinear response and is red-shifted from the diagonal along the emission energy axis by the biexciton binding energy. The LP in Fig. 2(a) corresponds to the quantum path starting from the ground state shown in Fig. 1(c). In this work, we focus on neutral excitons and ignore trions. The polarization for the pre-pulse is set along the H direction, which transfers population from the ground state to the H exciton and from the H exciton to the biexciton. When the pre-pulse

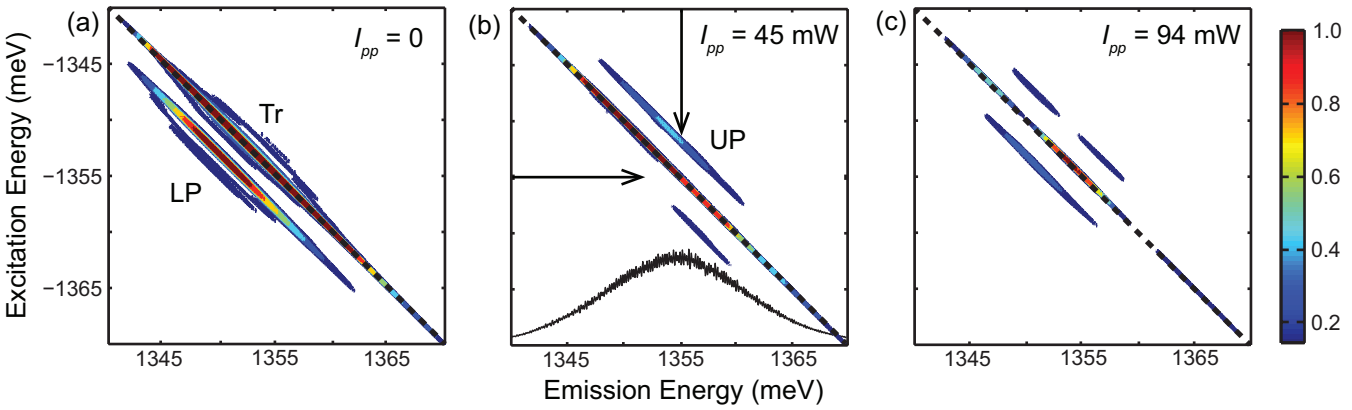

FIG. 2. (Color online) 2D rephasing amplitude spectra using pre-pulse power of (a) 0, (b) 45, and (c) 94 mW. Color corresponds to amplitude in the figures. The delay between the pre-pulse and 2DCS probe is 15 ps. The polarization for the pre-pulse is horizontal and for 2DCS is cross-linear (H-HVVH). The trion (Tr), lower (LP), and upper (UP) peaks are indicated. The inset in (b) shows a spectrum for the pre-pulse and each beam in 2DCS, and the arrows in (b) show resonant energy positions for the LP and UP, respectively.

is incident on the sample, other quantum paths starting with population in the H exciton state (Figs. 1(d) and 1(e)) and the biexciton state (Fig. 1(f)) also contribute to the 2D signal. The quantum path shown in Fig. 1(d) contributes to the signal at the position of the LP in the 2D spectrum with the opposite sign compared to the signal from Fig. 1(c). Similarly, signals from the quantum paths shown in Figs. 1(e) and 1(f) appear at the position labeled as the UP in Fig. 2(b), which is red-shifted from the diagonal along excitation energy axis by the biexciton binding energy, with opposite signs with respect to each other. As a result, the LP represents the difference between the ground state population ρ_{G} and the H exciton state population ρ_{H}, whereas the UP represents the difference between the H exciton population ρ_{H} and the biexciton state population ρ_{B}. It should be mentioned that the quantum paths starting from off-diagonal elements such as ρ_{GH} do not contribute to the signal due to the phase matching condition. Figures 2(b) and 2(c) are the 2D spectra at Δt = 15 ps for the pre-pulse powers I_{pp} of 45 and 94 mW, respectively. As I_{pp} increases, the LP disappears and the UP appears (Fig. 2(b)). However, as I_{pp} increases further, the LP re-appears and the UP disappears again (Fig. 2(c)). This power dependence measurement is repeated for Δt = 15, 50, and 100 ps.

As we mentioned, 2D spectra show the difference between populations, coherently generated by the pre-pulse, in each state. Figure 3(a) shows peak amplitudes for the LP (red circles) and the UP (blue squares) at energy positions resonant with the pre-pulse as a function of the square root of the pre-pulse power $\sqrt{I_{pp}}$, which is proportional to the pulse area defined by the integral of the product of dipole moment and electrical field with respect to time. We define the resonant energy such that the energy between the ground and H exciton state is the same as the center energy of the pre-pulse (1355 meV). The resonant energies with the pre-pulse for the LP and UP correspond to 1355 meV at the excitation and emission energy axes, respectively, as shown by arrows in Fig. 2(b). The pre-pulse delay time is indicated at each panel in Fig. 3(a). At Δt = 15 ps, population relaxation can be ignored, since the lifetime of QD excitons and biexcitons is more than an order of magnitude longer. On the other hand, as Δt increases to 50 and 100 ps, population dynamics after coherent interaction with the pre-pulse affects the signal significantly, and both LP and UP become less sensitive to the pre-pulse power – for the same pre-pulse power, the change of the LP and UP amplitudes is reduced.

To quantify this behavior, we performed calculation using the optical Bloch equations (OBEs) for the 4-level system shown in Fig. 1(b), which is an extension of the OBEs for a 2-level system [31, 32]. The strength of coherent interaction with the pre-pulse and the population decay dynamics afterwards are characterized by the transition dipole moments μ_{ij} and population decay times T_{ij} between the states (i, j = G, H, V, B; $i \neq j$) shown in Fig. 1(b), which are chosen to reproduce the experimental data. Since the population decay rate of InAs self-assembled QDs at low temperature is known to be limited by the radiative lifetime [28], the population decay rates are inversely proportional to the square of the transition dipole moments,

$$\frac{1}{T_{ij}} \propto \mu_{ij}^2. \tag{1}$$

Each value used in the simulation is found in [32]. We ignore the spin relaxation between the H and V exciton states because the relevant time scale, at low temperature, is much greater than the delays used in this study [37]. Figure 3(b) shows the simulation results for population of each component as a function of the pulse area at

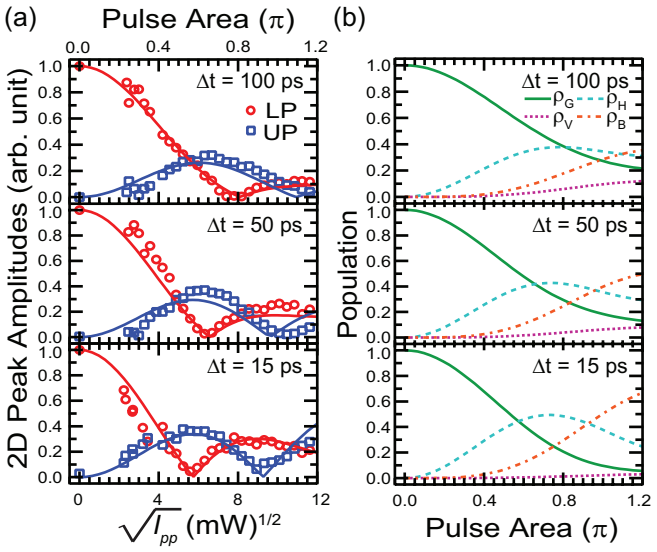

FIG. 3. (Color online) (a) Peak amplitudes of H pre-pulsed 2D rephasing spectra (H-HVVH) for the LP (red circles) and UP (blue squares).Solid lines are simulation results of $|\rho_G - \rho_H|$ (red) and $|\rho_H - \rho_B|$ (blue).The bottom axes are for data, whereas the top axes are for simulation results. (b) Simulation results for population in each state, ρ_G (solid), ρ_H (dashed), ρ_V (dotted), and ρ_B (dot-dashed).

each delay after the H polarized pre-pulse interacts with the 4-level system. The population differences $|\rho_G - \rho_H|$ and $|\rho_H - \rho_B|$ are also plotted as red and blue solid lines, respectively, in Fig. 3(a). The pulse area is defined such that a complete population inversion occurs between the ground and H exicton states ($\rho_G = 0$ and $\rho_H = 1$), in the absence of the biexciton state and population decay, when the pulse area is π. At $\Delta t = 15$ ps, as the pulse area increases, population transfer occurs through the coherent interaction from the ground to H exciton states and ρ_H exceeds ρ_G at the pulse area of around 0.55 π, where $|\rho_G - \rho_H| = 0$. In a 2D rephasing amplitude spectrum, that corresponds to Fig. 2(b). As the pulse area increases further, ρ_H starts becoming lower at around 0.7 π. In contrast, ρ_B keeps growing and exceeds ρ_H at the pulse area of around 1.0 π (Fig. 2(c)). As Δt increases, the population transfer from the biexciton to H and V exciton states as well as from the H and V exciton to ground states occurs through radiative decays, and it is clearly shown in the simulation results that significant amount of ρ_B and ρ_H are transferred to ρ_V and ρ_G for higher pulse areas.

To confirm the validity of these results, we perform experiments and simulations with a V polarized pre-pulse (V-HVVH), in which case the H exciton state cannot be populated through coherent interaction with the pre-pulse. As a result, the quantum paths starting with population in the H exciton state (Figs. 1(d) and 1(e)) do not contribute to the signal, shortly after the interaction with the pre-pulse. Figures 4(a) and 4(b) show the 2D spectra for I_{pp} of 40 and 126 mW, respectively, at Δt = 15 ps. Since the 2D spectra for $I_{pp} = 0$ is the same as Fig. 2(a), we do not show it again. With increasing I_{pp}, the 2D spectra exhibit a contrasting trend; the decrease of the LP and the increase of the UP happens at a slower rate. Experiments at $\Delta t = 50$ and 100 ps are also conducted. Figure 4(c) shows 2D peak amplitudes of the LP (red circles) and UP (blue squares) at the resonant energies as a function of $\sqrt{I_{pp}}$ at indicated Δt. As we mentioned, at short time delay ($\Delta t = 15$ ps), the LP and UP represent ρ_G and ρ_B, respectively, due to the absence of H excitons. As Δt increases, both the LP and UP become less sensitive to the pre-pulse power.

By changing the polarization of the pre-pulse, we observe different behaviors of population dynamics, which are consistent with the quantum pathways. The simulation results for the interaction with the V polarized pre-pulse are also shown in Figs. 4(c) and 4(d) in the same manner as Figs. 3(a) and 3(b). The characteristic feature of the V polarized pre-pulse at larger Δt and higher pulse area is that a noticeable amount of ρ_H is created through the radiative decay process, which results in the reduction of 2D peak amplitudes of both UP and LP at larger pulse area. Although experimental results correspond to population differences, we can obtain population in each state by comparing with calculation results.

In summary, we demonstrate coherent control of the exciton/biexciton system in an ensemble of $\sim 10^7$ InAs self-assembled QDs, and show the ability of reading out population in each state using 2DCS. We obtained an excellent agreement between the experiments and theory. The technique and information obtained in this work are of interest in the field of QD SOAs, where coherent light-matter interactions have been used to control the quantum state of ensemble QDs [11, 38]. This work also demonstrates the potential of 2DCS as a probe of excited states in other inhomogeneously broadened system [39, 40].

The work at JILA was primarily supported by the Chemical Sciences, Geosciences, and Energy Biosciences Division, Office of Basic Energy Science, Office of Science, U.S. Department of Energy under Award No. DE-FG02-02ER15346. T. S. acknowledges support by Japan Society for the Promotion of Science (JSPS). A.D.W. gratefully acknowledges support of Mercur Pr-2013-0001, DFG-TRR160 Z1, BMBF - Q.com-H 16KIS0109, and the DFH/UFA CDFA-05-06.

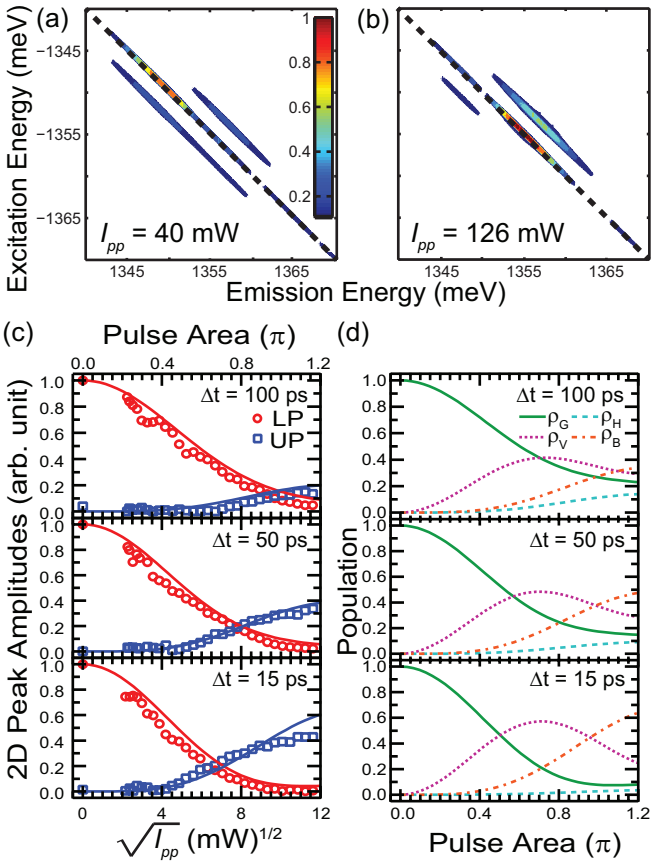

FIG. 4. (Color online) (a) Vertically polarized pre-pulse 2D rephasing amplitude spectra (V-HVVH) at prepulse power of (a) 40 and (b) 126 mW at $\Delta t = 15$ ps. (c) Peak amplitudes of V-HVVH for LP (red circles) and UP (blue squares).Solid lines are simulation results of $|\rho_G - \rho_H|$ and $|\rho_H - \rho_B|$.The bottom axes are for data, whereas the top axes are for simulation results. (d) Simulation results for population in each state, ρ_G (solid), ρ_H (dashed), ρ_V (dotted), and ρ_B (dot-dashed).

[1] Y. Kubo, F. R. Ong, P. Bertet, D. Vion, V. Jacques, D. Zheng, A. Dréau, J. -F. Roch, A. Auffeves, F. Jelezko, J. Wrachtrup, M. F. Barthe, P. Bergonzo, and D. Esteve, Phys. Rev. Lett. **105**, 140502 (2010).

[2] Y. O. Dudin, L. Li, F. Bariani, and A. Kuzmich, Nat. Phys. **8**, 790 (2012).

[3] A. P. Alivisatos, A. L. Harris, N. J. Levinos, M. L. Steigerwald, and L. E. Brus, J. Chem. Phys., **89**, 4001 (1988).

[4] D. T. Nguyen, C. Voisin, Ph. Roussignol, C. Roquelet, J. S. Lauret, and G. Cassabois, Chem. Phys. **413**, 102 (2013).

[5] *Quantum Dots-Optics, Electron Transport and Future Applications*, edited by Alexander Tartakovskii (Cambridge University Press, New York, 2012).

[6] T. H. Stievater, Xiaoqin Li, D. G. Steel, D. Gammon, D. S. Katzer, D. Park, C. Piermarocchi, and L. J. Sham, Phys. Rev. Lett. **87**, 133603 (2001).

[7] H. Kamada, H. Gotoh, J. Temmyo, T. Takagahara, and H. Ando, Phys. Rev. Lett. **87**, 246401 (2001).

[8] A. J. Ramsay, Semicond. Sci. Technol. **25**, 103001 (2010).

[9] Y. Arakawa and H. Sakaki, Appl. Phys. Lett. **40**, 939 (1982).

[10] D. L. Huffaker, G. Park, Z. Zou, O. B. Shchekin, and D. G. Deppe, Appl. Phys. Lett. **73**, 2564 (1998).

[11] M. Korarczik, N. Owschimikow, J. Korn, B. Lingnau, Y. Kaptan, D. Bimberg, E. Schöll, K. Lüdge, and U. Woggon, Nature Commun. **4**, 2953 (2013).

[12] J. J. Finley, M. Skalitz, M. Arzberger, A. Zrenner, G. Böhm, and G. Abstreiter, Appl. Phys. Lett., **73**, 2618 (1998).

[13] L. A. Rozema, D. H. Mahler, A. Hayat, P. S. Turner, and A. M. Steinberg, Phys. Rev. Lett. **113**, 160504 (2014).

[14] J. J. Berry, M. J. Stevens, R. P. Mirin, and K. I. Silverman, Appl. Phys. Lett. **88**, 061114 (2006).

[15] L. Yang, P. Glasenapp, A. Greilich, D. Reuter, A. D. Wieck, D. R. Yakovlev, M. Bayer, and S. A. Crooker, Nature Commun. **5**, 4949 (2014).

[16] P. Borri, W. Langbein, S. Schneider, U. Woggon, R. L. Sellin, D. Ouyang, and D. Bimberg, Phys. Rev. Lett. **87**, 157401 (2001).

[17] P. Borri and W. Langbein, J. Phys. Condens. Matter **19**, 295201 (2007).

[18] G. Moody, R. Singh, H. Li, I. A. Akimov, M. Bayer, D. Reuter, A. D. Wieck, and S. T. Cundiff, Phys. Rev. B **87**, 045313 (2013).

[19] M. E. Siemens, G. Moody, H. Li, A. D. Bristow, and S. T. Cundiff, Opt. Express **18**, 17699 (2010).

[20] G. Moody, M. E. Siemens, A. D. Bristow, X. Dai, D. Karaiskaj, A. S. Bracker, D. Gammon, and S. T. Cundiff, Phys. Rev. B **83**, 115324 (2011).

[21] G. Moody, R. Singh, H. Li, I. A. Akimov, M. Bayer, D. Reuter, A. D. Wieck, A. S. Bracker, D. Gammon, and S. T. Cundiff, Phys. Rev. B **87**, 041304(R) (2013).

[22] P. Borri, W. Langbein, S. Schneider, U. Woggon, R. L. Sellin, D. Ouyang, and D. Bimberg, Phys. Rev. B **66**, 081306(R) (2002).

[23] M. Kujiraoka, J. Ishi-Hayase, K. Akahane, N. Yamamoto, K. Ema, and M. Sasaki, Appl. Phys. Express **3**, 092801 (2010).

[24] Y. R. Shen, *The Principles of Nonlinear Optics*, (Wiley-Interscience, New York, 1984).

[25] A. D. Bristow, D. Karaiskaj, X. Dai, T. Zhang, C. Carlsson, K. R. Hagen, R. Jimenez, and S. T. Cundiff, Rev. Sci. Instrum. **80**, 073108 (2009).

[26] S. Rodt, A. Schliwa, R. Heitz, V. Türck, O. Stier, R. L. Sellin, M. Strassburg, U. W. Pohl, and D. Bimberg, Phys. Stat. Solidi B **234**, 354 (2002).

[27] M. Bayer, G. Ortner, O. Stern, A. Kuther, A. A. Gorbunov, A. Forchel, P. Hawrylak, S. Fafard, K. Hinzer, T. L. Reinecke, S. N. Walck, J. P. Reithmaier, F. Klopf, and F. Schäfer, Phys. Rev. B **65**, 195315 (2002).

[28] W. Langbein, P. Borri, U. Woggon, V. Stavarache, D. Reuter, and A. D. Wieck, Phys. Rev. B **70**, 033301 (2004).

[29] G. Moody, R. Singh, H. Li, I. A. Akimov, M. Bayer, D. Reuter, A. D. Wieck, and S. T. Cundiff, Solid State Commun. **163**, 65 (2013).

[30] P. S. Sokolov, M. Y. Petrov, T. Mehrtens, K. Müller-Caspary, A. Rosenauer, D. Reuter, and A. D. Wieck, Phys. Rev. B **93**, 045301 (2016).

[31] L. Allen and J. H. Eberly, *Optical Resonance and Two-Level Atoms*, (Dover Publications Inc., New York, 1987).

[32] See Supplemental Material, which includes Refs. [33-36].

[33] Shaul Mukamel, *Principles of Nonlinear Optical Spectroscopy*, (Oxford University Press, New York, 1995).

[34] Robert W. Boyd, *Nonlinear Optics*, (Academic Press, Orlando, 2008).

[35] S. J. Boyle, A. J. Ramsay, F. Bello, H. Y. Liu, M. Hopkinson, A. M. Fox, and M. S. Skolnick, Phys. Rev. B **78**, 075301 (2008).

[36] M. Wimmer, S. V. Nair, and J. Shumway, Phys. Rev. B **73**, 165305 (2006).

[37] M. Paillard, X. Marie, P. Renucci, T. Amand, A. Jbeli, and J. M Gérard, Phys. Rev. Lett. **86**, 1634 (2001).

[38] O. Karni, A. K. Mishra, G. Eisenstein, and J. P. Reithmaier, Phys. Rev. B **91**, 115304 (2015).

[39] T. Brixner, J. Stenger, H. M. Vaswani, M. Cho, R. E. Blankenship, and G. R. Fleming, Nature (London) **434**, 625 (2005).

[40] V. M. Huxter, T. A. A. Oliver, D. Budker, and G. R. Fleming, Nat. Phys. **9**, 744 (2013).